Molecular Cell, Vol. 16, 351–362, November 5, 2004, Copyright ©2004 by Cell Press

Structure of the *Tetrahymena* Ribozyme: Base Triple Sandwich and Metal Ion at the Active Site

Feng Guo,[1] Anne R. Gooding, and Thomas R. Cech*
Howard Hughes Medical Institute
Department of Chemistry and Biochemistry
University of Colorado
Boulder, Colorado 80309

Summary

The *Tetrahymena* intron is an RNA catalyst, or ribozyme. As part of its self-splicing reaction, this ribozyme catalyzes phosphoryl transfer between guanosine and a substrate RNA strand. Here we report the refined crystal structure of an active *Tetrahymena* ribozyme in the absence of its RNA substrate at 3.8 Å resolution. The 3′-terminal guanosine (ωG), which serves as the attacking group for RNA cleavage, forms a coplanar base triple with the G264-C311 base pair, and this base triple is sandwiched by three other base triples. In addition, a metal ion is present in the active site, contacting or positioned close to the ribose of the ωG and five phosphates. All of these phosphates have been shown to be important for catalysis. Therefore, we provide a picture of how the ribozyme active site positions both a catalytic metal ion and the nucleophilic guanosine for catalysis prior to binding its RNA substrate.

Introduction

The *Tetrahymena* preribosomal RNA intron, which undergoes self-splicing in the absence of any proteins (Kruger et al., 1982), was the first example of a ribozyme. It was soon recognized to be a member of the group I intron family (Davies et al., 1982; Michel and Dujon, 1983), more than 1500 examples of which are now known (Cannone et al., 2002). Many other classes of RNA catalysts have now been found from natural sources or from in vitro selection experiments, including the protein synthesis machinery (the ribosome) and presumably the pre-mRNA splicing machinery (the spliceosome) (Doudna and Cech, 2002; Guerrier-Takada et al., 1983; Joyce, 2004; Nissen et al., 2000; Valadkhan and Manley, 2001). These ribozymes use various strategies for catalysis. For example, the hairpin ribozyme employs several nucleobases for transition state stabilization (Rupert et al., 2002). In contrast, the *Tetrahymena* ribozyme has been proposed to use metal ions to activate the nucleophile and otherwise stabilize the transition state (Piccirilli et al., 1993; Shan et al., 1999a).

The *Tetrahymena* ribozyme has been a paradigm for the study of RNA catalysis. Extensive biochemical and genetic studies have elucidated the basic catalytic mechanism (Figure 1). The intron portion of the RNA precursor (i) first binds an exogenous guanosine (ii), which then attacks the 5′ splice site and becomes covalently attached to the 5′ end of the intron (iii). Subsequently, the ribozyme undergoes a conformational change, during which the 3′-terminal guanosine (ωG) binds in the G-site. This results in the positioning of the 3′ splice site for nucleophilic attack by the 3′-OH of the 5′ exon (iv), accomplishing precise ligation of the exons (v). Following the release of the ligated exons, a 5′ region of the intron can fold back into the active site and become a substrate for a third nucleophilic attack (vi), by ωG. This produces a circularized intron (vii) and releases an RNA oligo with the exogenous G attached at the 5′ end.

Like a protein enzyme, the ribozyme needs to form a highly specific three-dimensional structure to catalyze this series of precise reactions. Thus, structural biology has become a focus of the group I intron field. In 1996, the crystal structure of a self-folded domain of the *Tetrahymena* ribozyme, called the P4-P6 domain, was determined at 2.8 Å resolution (Cate et al., 1996). This structure demonstrated how a large RNA structure is closely packed, but did not include the catalytic residues. Later, an engineered, active *Tetrahymena* ribozyme (named Tet3-9) was crystallized and its structure was solved at 5.0 Å resolution (Golden et al., 1998). This model indicated that the ribozyme active site is largely preorganized for catalysis even in the absence of the RNA substrate. However, due to the limitation of the resolution, the structure was not refined against the diffraction data and many molecular details could not be determined. Very recently, the crystal structure of a group I intron from the pretransfer RNA of the bacterium *Azoarcus* with both exons bound was determined at 3.1 Å resolution (Adams et al., 2004). In this work, Strobel and colleagues demonstrated how the active site of the ribozyme is organized at state iv in the self-splicing pathway. Given the multiple states shown in Figure 1, clearly a number of crystal structures will be required to make a molecular movie of the complete RNA splicing reaction.

We have been using in vitro selection to identify thermostable variants of RNAs, with the hope that they would form more organized crystal lattices and have improved diffraction limits. In one case, selection identified a single-base deletion of the P4-P6 domain (Juneau and Cech, 1999) that improved the diffraction limit of the crystals from 2.8 to 2.25 Å resolution (Juneau et al., 2001). Subsequently, selection of a library of mutant *Tetrahymena* ribozymes for both thermostability and activity identified nine mutations that increased the stability by 10.5°C and retained catalytic function at elevated temperatures (Guo and Cech, 2002).

Here we introduce these stabilizing mutations into the ribozyme crystallized earlier (five of the nine mutated sites are present in the construct of Golden et al. [1998]); the new ribozyme (named Tet3-9-R14C) cleaves an RNA substrate in *trans* using its ωG (Figure 1, viii–x). The variant ribozyme not only still crystallizes but also has a substantially improved diffraction limit. We describe the crystal structure of this active *Tetrahymena* ribo-

*Correspondence: thomas.cech@colorado.edu
[1]Present address: Department of Biological Chemistry, University of California, Los Angeles School of Medicine, Box 951737, Los Angeles, California 90095.

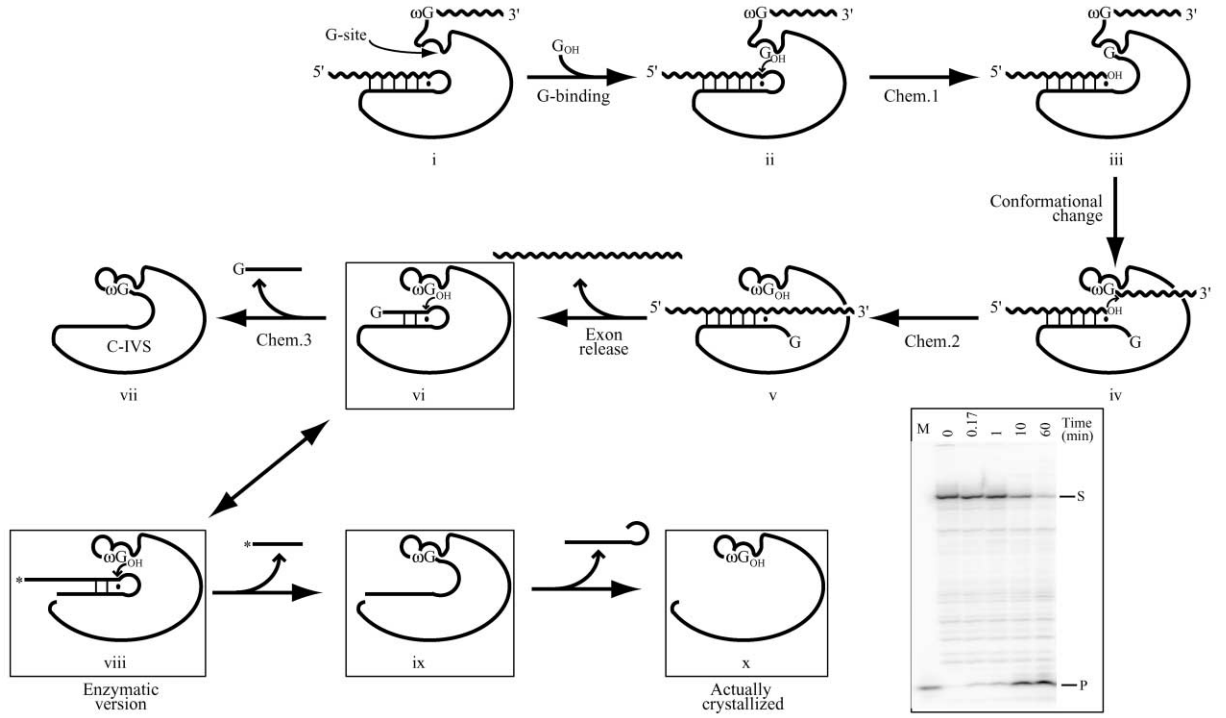

Figure 1. The Group I Intron Splicing Mechanism and Its Related Enzymatic Activity

Self-splicing begins with the binding of an exogenous molecule of guanosine or one of its 5′-phosphorylated derivatives (G_{OH}, where the subscript represents the free 3′-OH group). The G-site is located in paired region P7 of all group I introns. The reaction proceeds through three chemical steps with release of a short oligo with the exogenous G linked at its 5′ end (Chem.3). Wavy lines represent the 5′ and 3′ exons and thick lines stand for the intron. Watson-Crick and G:U wobble base pairs are indicated by thin bars and dots, respectively. The enzymatic form of the ribozyme (viii) closely resembles form vi, which is the product of the exon ligation step of splicing and the precursor for intron circularization. The crystallized ribozyme (x) is the enzymatic form in the absence of its substrate. The cleavage activity (from viii to ix) of this ribozyme under crystallization conditions is shown in the insert. The substrate (S) includes nucleotides in the paired regions 1, 2, and 2.1. The cleavage product (P) terminates at the 5′ splice site. M is a synthetic marker chemically identical to the product.

zyme in the absence of its RNA substrate at 3.8 Å resolution. The improved resolution allows the elucidation of the active site configuration prior to the association of the substrate. The ωG is bound in the G-site in one of four layers of base triples. A catalytic magnesium ion is proposed to bind in the active site, based on a heavy atom soak experiment. This work provides a refined crystal structure of an active *Tetrahymena* ribozyme.

Results

Crystallization and Structure Determination

Introduction of the five stabilizing mutations into Tet3-9 improved the diffraction of the ribozyme crystals to 3.8 Å resolution. The improvement in diffraction critically depended on soaking the ribozyme crystals in stabilizer solutions containing 15% ethanol. During this process, the space group of the crystals changed from $P4_22_12$ to $P4_12_12$, and the cell constant along the c axis increased from around 200 to 304 Å (see Experimental Procedures for details).

The crystals were not isomorphous with each other and decayed severely during data collection at synchrotron X-ray sources. Thus, about 120 data sets were collected in the course of the project. The structure was finally solved by combining phase information derived from several single anomalous dispersion (SAD) data sets on Eu, Dy, and iridium hexammine (Ir) derivatives and a multiwavelength anomalous dispersion (MAD) data set on an Ir derivative (Table 1). After large parts of the P4-P6 domains were traced, the model phases greatly improved the quality of the electron density. The final structure contains four independent ribozyme molecules with 968 out of 988 residues ordered.

At 3.8 Å resolution, the phosphate positions are normally well determined (Figure 2). The base positions are clearly visible in the electron density in some regions, but are continuous with neighboring bases in others. Assuming A-form structures, the residues in helical regions are better determined than those in single strands.

Overall Structure

The four independent monomeric structures corresponding to the four molecules in the asymmetric unit have most of their structural features in common (Figure 3; see Supplemental Table S1 at http://www.molecule.org/cgi/content/full/16/3/351/DC1/). For example, the A and B molecules have an rms deviation of 1.4 Å for all the residues that are ordered in both structures (242 out of a total of 247 nt). The P4-P6 domains and the P3 and P7 helices are the most superimposable regions, with rms deviations ranging from 1.1 to 2.0 Å between the

Table 1. Summary of Crystallographic Analysis

Data Collection Statistics[a]									
	Native	Eu	Ir-1	Dy-1	Dy-2	Dy-3	Ir-2	Ir-3	Ir-4
Resolution	3.8 Å	6.0 Å	5.5 Å	5.2 Å	6.2 Å	6.2 Å	5.5 Å	5.5 Å	5.5 Å
Wavelength	1.0332Å	1.7758Å	1.1052 Å	1.5906 Å	1.5912 Å	1.5514 Å	1.1056 Å	1.1053 Å	1.0862Å
R_{merge}	8.8%	7.9%	7.8%	9.2%	8.7%	8.1%	8.8%	8.6%	8.6%
	(27.2%)	(47.3%)	(42.2%)	(70.5%)	(75.3%)	(64.5%)	(50.7%)	(44.1%)	(42.3%)
Completeness	93.9%	96.4%	93.0%	94.4%	96.4%	96.2%	92.5%	88.0%	87.6%
	(76.8%)	(94.0%)	(91.1%)	(90.9%)	(93.5%)	(92.8%)	(90.1%)	(78.1%)	(81.1%)
I/σ	24.0	18.4	17.8	12.2	12.9	13.7	14.4	13.6	13.7
	(3.6)	(3.3)	(3.0)	(1.8)	(1.7)	(2.1)	(2.0)	(1.9)	(1.9)
Redundancy	4.8	4.3	3.3	3.0	3.1	3.1	2.8	2.5	2.5
	(1.8)	(4.0)	(3.0)	(2.7)	(2.8)	(2.8)	(2.0)	(1.3)	(1.4)
Phasing Statistics									
Method		SAD	SAD	SAD	SAD	SIR (Dy-2/Dy-3)		MAD (Ir-2,3,4)	
Resolution		6.0 Å	5.5 Å	5.2 Å	6.4 Å	8.0 Å		5.5 Å	
Number of sites		39[b]	28[b]	28	28	28		17	
Phasing power		2.0	1.4	1.9	1.4	1.4	1.7	1.7	1.2
Figure of merit		0.32	0.22	0.29	0.23	0.35		0.43	
Phase combination			Eu/Ir-1			Dy-1,2,3/Ir-2,3,4			
Resolution			5.5 Å			5.2 Å			
Figure of merit			0.32			0.45			
Refinement Results									
Resolution	20–3.8 Å (3.97–3.80 Å)								
R_{work}	0.263 (0.345)								
R_{free}	0.320 (0.391)								
No. of Reflections	43,972								
	Bond Lengths	Bond Angles							
Rmsd	0.008 Å	1.4°							

[a] Each statistical value in parentheses was obtained from the highest resolution shell of the corresponding data set.
[b] The heavy atom sites of Eu and Ir-1 include weak ones that were identified using model phases.

four molecules. The conclusions described in this work are true for at least three molecules unless otherwise stated. Large differences between the four structures appear to be localized to specific peripheral regions, such as the P9 and P8 helices (Figure 3C; Supplemental Figure S1A). In particular, P9 and neighboring regions of molecule C are located far from the equivalent regions in the other three molecules; this occurs because the interaction between L9 and the P5 and J5/5a regions seen in the other three molecules is disrupted by a crystal contact.

Our higher resolution ribozyme structure confirms the overall architecture of the previous 5 Å resolution model (Golden et al., 1998). The P4-P6 domain forms a hairpin-like structure, consisting of two pseudocontinuous helical regions connected by a sharp bend. This part of the structure is similar to the crystal structure of the isolated domain (Cate et al., 1996), with some differences in the loop regions between P6 and P6a (discussed below). The P3 and P8 helices are coaxially stacked. The three nucleotides in the joint region between P7 and P3 (J7/3) introduce a bend between these neighboring helices. P9 is oriented 90° from P7. The P3-P9 domain wraps around the P4-P6 domain through extensive interdomain interactions to form the active site of the ribozyme (Figure 3B).

The largest differences between the new Tet3-9-R14C model and the previous Tet3-9 model originate from the P3-P9 domain regions as indicated by a difference distance matrix plot analysis (Richards and Kundrot, 1988) (Supplemental Figure S1B). For example, residues 261–275 in the P7 and P3 regions appear to follow the same path in their superposition, but differ in register by 1–2 residues. The difference may be an indication of the limitation of the low-resolution model. Alternatively, the five mutations introduced into Tet3-9-R14C and the different crystalline environments may contribute to the differences.

New Views of Tertiary Interactions

The higher resolution structure provides detailed views of tertiary interactions involving P6. The A104 residue uses its minor groove surface and the 2′-OH of the ribose to contact the ribose of C217; the structure here is similar to the type II A-minor interaction (Doherty et al., 2001), even though C217 is not involved in a classic Watson-Crick base pair. The A105 residue uses its minor groove side of the base and ribose to contact the entire minor groove surface of the C216-G257 pair in P6, forming a type I base triple interaction (Figure 3D). Together, these two interactions constitute a consecutive type I/II motif (Doherty et al., 2001). The U106 residue interacts with the U258 ribose directly using its ribose moiety, and likely with direct or water-mediated hydrogen bonds

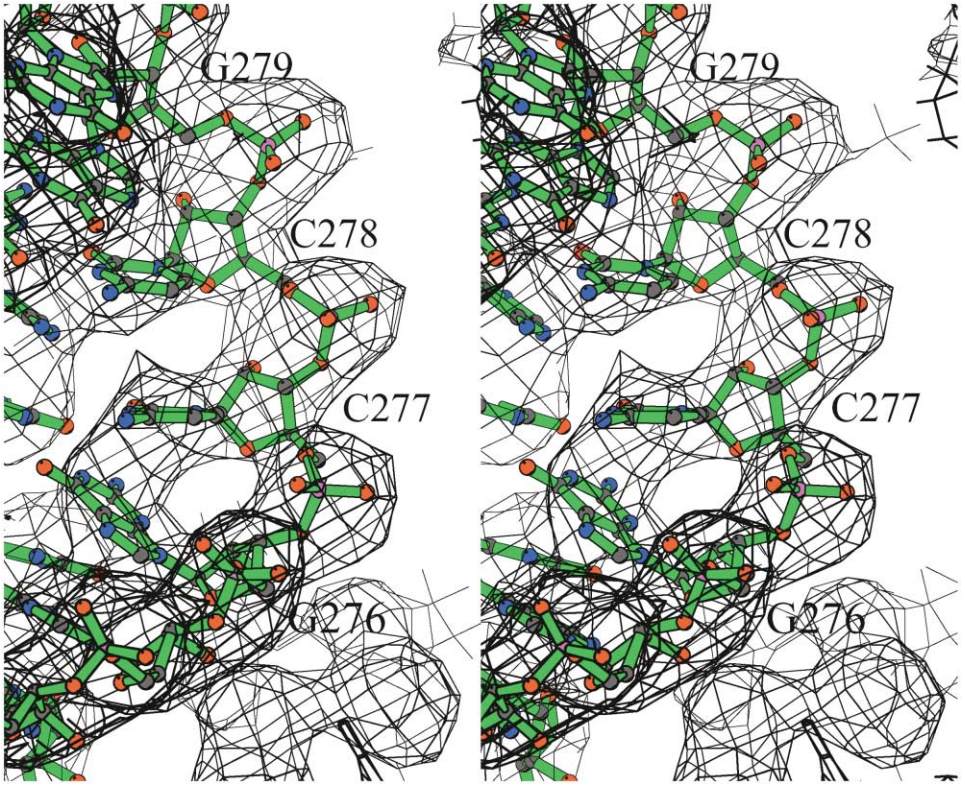

Figure 2. Stereoview Showing a Portion of the $2F_o - F_c$ Composite Omit Map
Electron density is contoured at 1.0 σ cutoff.

involving the U106 base. Overall, this J3/4 region appears to form a "triple-helical scaffold" with P6 as predicted by Michel et al. (Michel et al., 1990a; Michel and Westhof, 1990), although the position and orientation of the J3/4 residues are quite different. The native conformation of this region was not visible in the isolated P4-P6 structure (Cate et al., 1996), because of a crystal contact and interactions with two unnatural guanosines added to facilitate transcription.

The symmetric internal loop between P6 and P6a now adopts a conformation different from the isolated P4-P6 domain structure and also different from the 5 Å Tet3-9 model. The bases of C217 and C255 form a single hydrogen bond base pair, leaving a bulged adenosine residue at each end. The bulged A218 interacts with C102-G272 through a type II A-minor base triple. The base of A256 contacts the backbones of G272 and U273. Both of these contribute to connecting the two major domains of the ribozyme (magenta lines in Figure 3A), a previously unrecognized function.

The L9 loop is involved in an interdomain interaction with the P5 and J5/5a regions. The A324 base in L9 stacks with the A125 base in the J5/5a region. The A325 residue forms a type II A-minor interaction with G119-U202.

Guanosine Bound in a Triple-Helical Sandwich

The 3′-terminal guanosine of the ribozyme binds similarly to the P7 G binding site in all four molecules. The G binding site is composed of four layers of base triples (Figure 4 and Supplemental Figure S2). In an early study, Michel et al. provided evidence that the exogenous guanosine forms a major-groove base triple with the G264-C311 pair (Michel et al., 1989). Subsequently, Been and Perrotta found that the 3′-terminal G is bound in the same site (Been and Perrotta, 1991). The hydrogen bonding interactions proposed in these studies are the same as what we observe in the crystal structure.

The ωG·G264-C311 triple is sandwiched by three other layers of base triples. Above the ωG-triple in Figure 4A, C262 pairs with G312 as expected from the phylogenetically derived secondary structure. However, A263, which is depicted as a bulged residue in secondary structure diagrams, forms two hydrogen bonds to the minor groove side of G312 (Figures 4B and 4D); this feature was predicted in the Axial III model of Yarus et al. (Yarus et al., 1991). The base of C262 is located right above the purine ring of ωG, presumably stabilizing its binding by base stacking. Below the ωG-triple, the A261 base contacts the major groove of the A265-U310 pair (Figure 4E). In a further layer, the Hoogsteen surface of the A306 base is close enough to the major groove of the C266-G309 pair that another base triple is possible. The last base triple is also supported by phylogenetic data (Michel and Westhof, 1990). The backbone connecting A261 and C262 adopts an extended conformation to span two steps of the P7 helix.

The P9.0 helix has been proposed to aid in 3′-splice site recognition (Burke et al., 1990; Michel et al., 1990b). Only the C413-G313 base pair of P9.0 helix is observed in the Tet3-9-R14C structure. This pair may contribute

to guanosine binding by anchoring the strand close to the G binding pocket and stacking onto the A263·C262-G312 triple.

A Metal Ion Bound at the Active Site

Metal ions are not only required for the folding of the ribozyme but also play a direct role in catalysis (Draper, 2004; Fedor, 2002). It has been proposed based on metal ion rescue experiments that three magnesium ions are present at the active site of the ribozyme, to activate the nucleophile, stabilize the leaving group, and otherwise stabilize the transition state (Piccirilli et al., 1993; Shan et al., 1999a; Sjogren et al., 1997; Sontheimer et al., 1997; Weinstein et al., 1997). Structural knowledge of magnesium binding sites should greatly improve our understanding of this unique class of catalysts.

Although our structure's resolution is not sufficient for identification of magnesium ions, the Eu and Ir binding sites on the ribozyme provide evidence of their location. Previous high-resolution structural studies of the P4-P6 domain have established the correlation between lanthanide binding sites and magnesium binding sites with inner sphere coordination. Hexammine compounds are well established to mimic hexahydrated magnesium ion in association with large RNA molecules (Cate and Doudna, 1996; Cate et al., 1999), although they do not always bind identically (Juneau et al., 2001).

Model-phased anomalous Fourier difference maps were used to establish the final heavy atom models. There are 22 strong Eu sites (a lanthanide element) and 16 strong Ir sites (Figure 5). These heavy metal ion sites are assumed to be magnesium ions in the final native structural model (E1–E22 for Eu sites, F1–F16 for Ir sites). Although the presence of magnesium ions at these sites is not verified in the present work, some of them are well established in the P4-P6 domain studies (Cate et al., 1996; Juneau et al., 2001). The inclusion of the metal ions in the crystallographic refinement only reduces the R factors modestly (0.0037 for the free R factor and 0.0028 for the working R factor).

In each molecule, there is a magnesium ion (E17, E16, E7, and E22 for molecules A, B, C and D, respectively) in close contact with at least one of the two ribose hydroxyl groups of ωG (Supplemental Table S2). The 3′-OH of ωG is the attacking nucleophile in the cleavage reaction (Figure 1, viii). The 2′-OH of ωG also makes a critical contribution to catalysis (Bass and Cech, 1986), due to lowering the pKa of the adjacent 3′-OH and positioning the nucleophile for attack (Shan and Herschlag, 1999; Shan et al., 1999b). Both functional groups are known to coordinate catalytic magnesium ions (Sjogren et al., 1997; Sontheimer et al., 1997; Weinstein et al., 1997).

These catalytic magnesium ions are within direct contact distance to the phosphates of residues C262, U305, and A306 (Figure 6A and Supplemental Table S2). The phosphates of A207 and C208 face the active site and are about 4–7 Å away from the magnesium sites. These are likely the major functional groups the ribozyme uses to chelate the catalytic metal ions. In an early study, phosphorothioate substitution-interference identified 13 phosphate positions that are important to the guanosine addition step (Figure 1, ii–iii) in the *Tetrahymena* intron self-splicing reaction (Christian and Yarus, 1993). Their list includes all five phosphates that are close to the active site in our structure, providing biochemical support for our proposal that they bind and position a catalytic metal ion. Similarly, a lead-cleavage approach identified this same region (A263 and U305, *Tetrahymena* numbering) of a bacteriophage T4 group I intron as being involved in metal binding (Streicher et al., 1993).

The active sites of the four molecules were superimposed using the phosphorus atoms of residues 262, 305, and 306 and the C1′ atom of ωG, with rms deviations ranging from 0.3 to 0.6 Å (Supplemental Figure S3). The magnesium ions appear to associate with the ribozyme in an elongated region between the phosphates of C262 and U305. Consistent with this observation, in some molecules the anomalous density is slightly elongated between the phosphates of C262 and U305 (Figure 6A). Since the space is too tight to fit in two magnesium ions, we think that one metal ion might have two or more slightly different locations along this short path.

Discussion

The *Tetrahymena* ribozyme provided the first example of a folded RNA molecule binding a small molecule (guanosine) with high affinity and specificity (Bass and Cech, 1984). The key element of the G binding site was identified by Michel et al. (1989): a G-C base pair in helix P7, conserved among all 1500 group I introns, formed a base triple with the guanosine ligand. Yet the story was clearly incomplete, because about half the base pairs in any RNA helix are G-C pairs; they cannot all be high-affinity G binding sites! The ribozyme crystal structure presented here now solves the mystery of why the one G-C base pair in P7 is so special: it is surrounded by an elaborate array of three additional, adjacent base triples formed by the RNA structure, providing a platform for G binding. Given the importance of base stacking in nucleic acid stability, having the guanosine "sandwiched" in this manner presumably accounts for much of the binding affinity, while the Michel base triple provides specificity.

On another front, the finding that group I introns use divalent cations (Mg^{2+} or Mn^{2+}) for catalysis led to the question of how these metal ions are held into place. Protein enzymes that catalyze similar nucleotidyl- or phosphoryl-transfer reactions, such as DNA polymerases, 3′-5′ exonuclease, and alkaline phosphatase, mainly use acidic amino acid side chains (Asp and Glu) to position two catalytic metals (Steitz, 1999). The active site metal ion in the ribozyme crystal structure presented here appears to be coordinated to three separate phosphate groups, brought together by the RNA tertiary structure. Similar to a protein metalloenzyme, this metal is bound to the ribozyme even in the absence of substrate. Another catalytic metal ion (M_A) is proposed to bind to a phosphoryl oxygen of the RNA substrate (Shan et al., 1999a), so it is reasonable that it would not be present in the substrate-free form of the ribozyme crystallized here.

Similar Catalytic Core Structure and G-Site in *Tetrahymena* and *Azoarcus* Structures

The G binding site of the *Tetrahymena* ribozyme has a structure similar to that of the *Azoarcus* group I intron

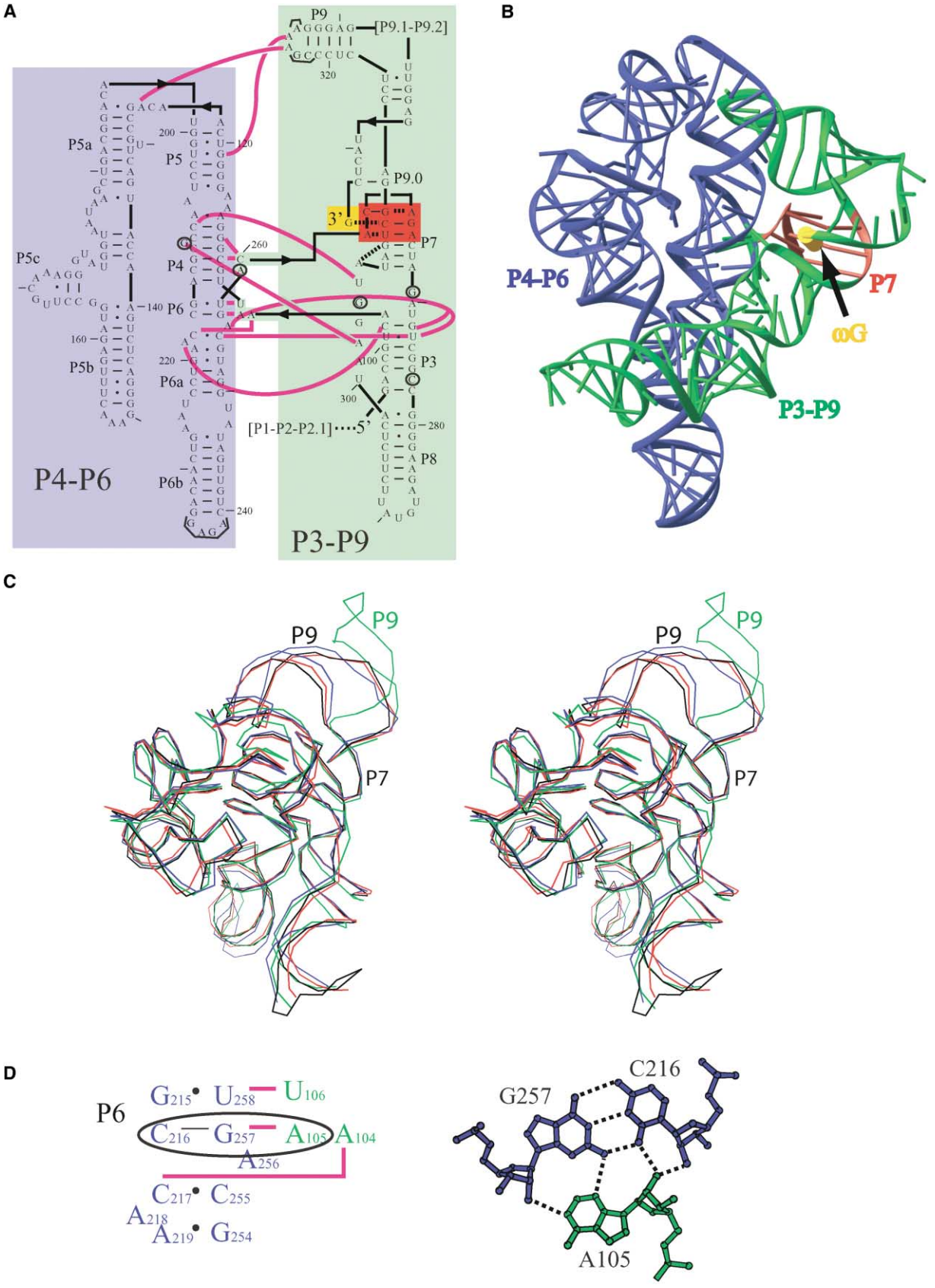

Figure 3. Structure of the *Tetrahymena* Ribozyme

(A) The secondary structure of the crystallized ribozyme. The P4-P6 and P3-P9 domains are indicated by blue and green backgrounds, respectively. The G binding site in base-paired region 7 (P7) is highlighted by a red background and 3′-terminal ωG in gold. The positions of

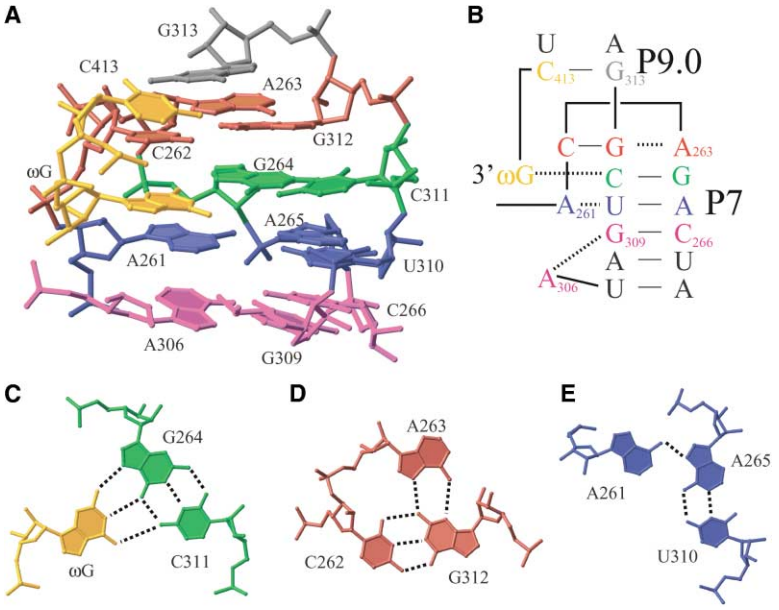

Figure 4. Structure of the Guanosine Binding Site

(A) Three-dimensional structure of the G-site in molecule B. The 3′-terminal ωG residue, which is the active site nucleophile, forms a coplanar base triple with the base pair G264-C311; this triple is sandwiched by three other triples colored as red, blue, and magenta, respectively.

(B) G-site secondary structure deduced from the crystal structure, using the same color scheme as in (A). Base triple interactions are shown as dashed lines.

(C) The base triple interactions between the ωG residue and the G264-C311 base pair.

(D) The base triple of A263, C262, and G312 above the ωG.

(E) The base triple of A261, A265, and U310 below the ωG.

in the presence of both exons (Adams et al., 2004). The C1′ atoms of the G-site residues from the two structures can be superimposed with an rms deviation of about 0.6 Å. Thus, the 3′-terminal G-OH (this structure) is bound the same as the 3′-splice site G, which has a 3′-phosphodiester bond (*Azoarcus* structure). Furthermore, the G binding site is structurally well organized in the absence of the bound RNA substrate (this structure) as in its presence (*Azoarcus* structure). This feature of the group I intron structures is consistent with the very modest thermodynamic coupling between the guanosine and RNA substrate binding (Bevilacqua et al., 1993; McConnell et al., 1993).

The core structures of the *Tetrahymena* and *Azoarcus* ribozymes are also quite similar to each other, despite the fact that they represent different structural subgroups of group I introns (1C1 and 1C3, respectively) and capture different catalytic stages. The C1′ atoms in the P3, P4, P6, and P7 regions can be superimposed with an rms deviation of 1.3 Å (the B molecule of Tet3-9-R14C was used). This observation argues that the catalytic core structure of group I introns may not undergo dramatic conformational rearrangements through steps iv–vi of self-splicing (Figure 1).

Potential Conformational Changes upon Substrate Binding

The relatively high sequence conservation (39 of 56 nt identical in the core) and the similar core structures between the *Tetrahymena* and *Azoarcus* ribozymes allow us to compare the two structures to infer conformational differences related to their reaction stages. The active sites of the *Tetrahymena* and *Azoarcus* ribozymes can be superimposed well using the C1′ atom of ωG and the phosphorus atoms of residues 262 and 306 (*Tetrahymena* numbering used throughout the text), with rms deviations of about 0.8 Å (Supplemental Figure S3B). However, in the *Azoarcus* structure, the phosphates of 207 and 208 are closer to the ωG and the catalytic metal ions; the phosphate of 208 occupies the position of that of 305 in the *Tetrahymena* structure. Although the base of 305 occupies a similar position in both structures, its ribose in *Azoarcus* is rotated along the glycoside bond to move the 305 phosphate far from the active site. Instead, the phosphate of 304 makes a contact with a metal ion. These conformational differences can originate from either the presence of the substrate or the different cleavage/ligation states of the two structures (the different linkages between ωG and the 3′-exon). Since both regions (207, 208 and 304, 305) interact with the substrate in the *Azoarcus* structure, the former possibility seems more likely.

Implications of the Prebound Metal Ion for Catalysis

Biochemical studies have suggested three distinct magnesium ions (termed M_A, M_B, and M_C) directly involved in group I intron catalysis (Shan et al., 1999a). In the transition state of the cleavage reaction by ωG, M_A coordinates to 3′-OH of U_{-1} (stabilizes the leaving group) and to the *pro-S*p nonbridging oxygen of the scissile phosphate (stabilizes the trigonal bipyramidal transition

the five stabilizing mutations are circled. The residues mutated to facilitate crystallization (Golden et al., 1998) are bracketed. Magenta lines represent interdomain interactions that are observed in at least three of the molecules in the asymmetric unit.

(B) RIBBONS diagram of the crystal structure of the ribozyme B molecule, with the same color scheme as in (A).

(C) Stereo C1′ traces of the four independent molecules in the crystal, superimposed with each other. Molecules A, B, C, and D are in red, black, green, and blue, respectively.

(D) A base triple interaction between the J3/4 (green) and P6 (blue) regions in molecule B. The secondary structure where this triple (highlighted by an oval) resides is shown on the left.

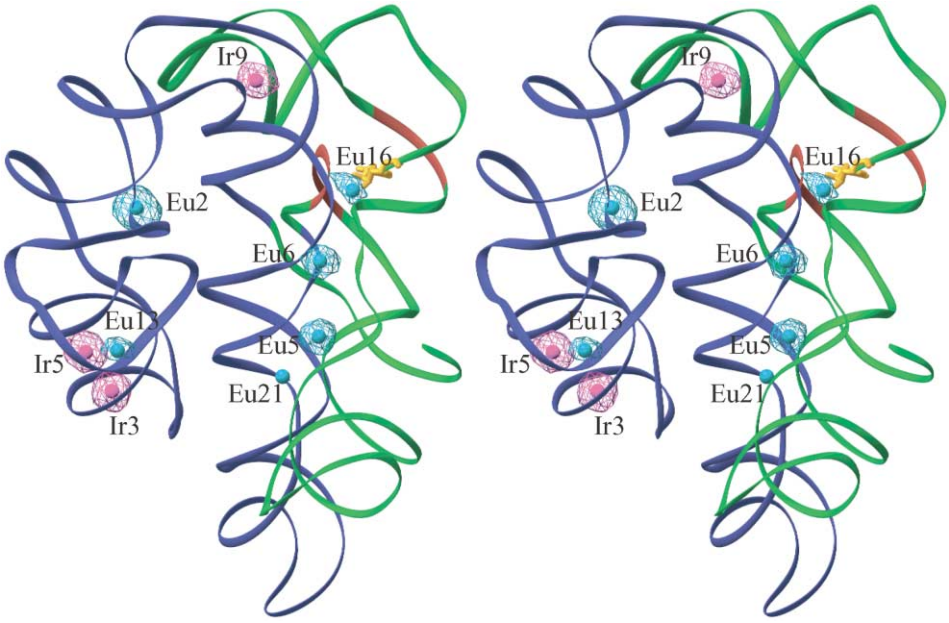

Figure 5. Stereo Representation of the Eu and Ir Sites in the Ribozyme

The model-phased anomalous Fourier's (Eu as cyan and Ir as magenta) are contoured at 6 σ cutoff. All four ribozyme molecules have similar Eu and Ir binding sites. The B molecule is shown in the figure. The ωG is drawn as gold and the G binding site as red. These heavy atom sites are assumed to be magnesium ions in the final refined native structure, with slight modifications to compensate for the nonisomorphism between crystals and to optimize the local coordination geometry.

state geometry) (Piccirilli et al., 1993; Yoshida et al., 1999); M_B coordinates to the 3′-OH of ωG (activates the nucleophile) (Sontheimer et al., 1997; Weinstein et al., 1997); and M_C coordinates to the 2′-OH of ωG and the *pro*-*S*p nonbridging oxygen (stabilizes the transition state geometry) (Sjogren et al., 1997).

Which catalytic metal ion corresponds to the observed active site ion? Based on its contact with the 3′- and 2′-OH of ωG, the observed magnesium ion can be either M_B or M_C. Furthermore, comparison with the *Azoarcus* structure suggests that it is M_C. Two metal ions (M_1 and M_2) are observed in the *Azoarcus* ribozyme structure (Adams et al., 2004). M_1, which is a magnesium ion, interacts with the phosphates of 208, 304, and 306, and the 3′-OH of the 5′-exon, as well as the *pro*-*S*p oxygen of the scissile phosphate. This metal ion is analogous to M_A in the biochemical model. M_2, which is a potassium ion, coordinates to the phosphates of 207, 262, and 306 and the 2′-OH of 261. M_2 is thought to be equivalent to M_C because of its proximity to the assumed 2′-OH of ωG in the *Azoarcus* structure. According to their coordinating partners, also taken into account the conformation differences described above, the divalent metal ion we observed is likely to be M_2 (or M_C) (Figure 6B).

On the other hand, the prebound magnesium ion in the ribozyme, in the absence of its RNA substrate, does not have to specifically be either of the catalytic metals. It is likely that, upon association with the substrate, the active site of the ribozyme undergoes conformational changes, which can in turn move this metal ion into its functional position for catalysis (Figure 6B) and presumably bring in two additional catalytic metal ions. Consistent with this view, the catalytic metal ion in the *Tetrahymena* structure occupies positions between M_1 and M_2 of the *Azoarcus* structure.

We now have three-dimensional structural information for two subclasses of group I introns and for only two of the multiple steps along the self-splicing pathway. Clearly the structural biology of these RNA catalysts will become even more interesting as the missing gaps are filled. Ultimately one would like to see a molecular movie of the entire series of reactions and to understand how group I introns with different secondary structures manage to accomplish the same splicing reaction.

Experimental Procedures

Cleavage Assays

The substrate used in the cleavage assays included residues −6 to 103 of the *Tetrahymena* ribosomal RNA precursor and was 5′ end labeled with ^{32}P. The procedure used in the assays was essentially the same as reported previously (Golden et al., 1997), except the reaction temperature was increased to 50°C and the reaction solution was exactly the same as the crystallization condition.

RNA In Vitro Transcription and Purification

The transcription template for Tet3-9-R14C RNA was cloned from the in vitro selected *Tetrahymena* L-21 R14C ribozyme (Guo and Cech, 2002), using the procedure described previously (Golden et al., 1997). The ribozyme was transcribed at 37°C by T7 RNA polymerase and purified using a denaturing tube gel electrophoresis system (Bio-Rad 491 Prep Cell and Biologic LP chromatography system). The eluted RNA was then concentrated, buffer-exchanged to 10 mM NaHEPES at pH 7.0, and stored at −20°C before crystallization.

Crystallization and Data Collection

The ribozyme solution used in crystallization contained 10 mg/ml RNA, 5 mM NaHEPES (pH 7.0), 10 mM NaCl, and 25 mM $MgCl_2$. For renaturation, 0.9 vol of solution containing 5.55 mM $MgCl_2$ and appropriate concentrations of RNA, buffer, and monovalent salt was

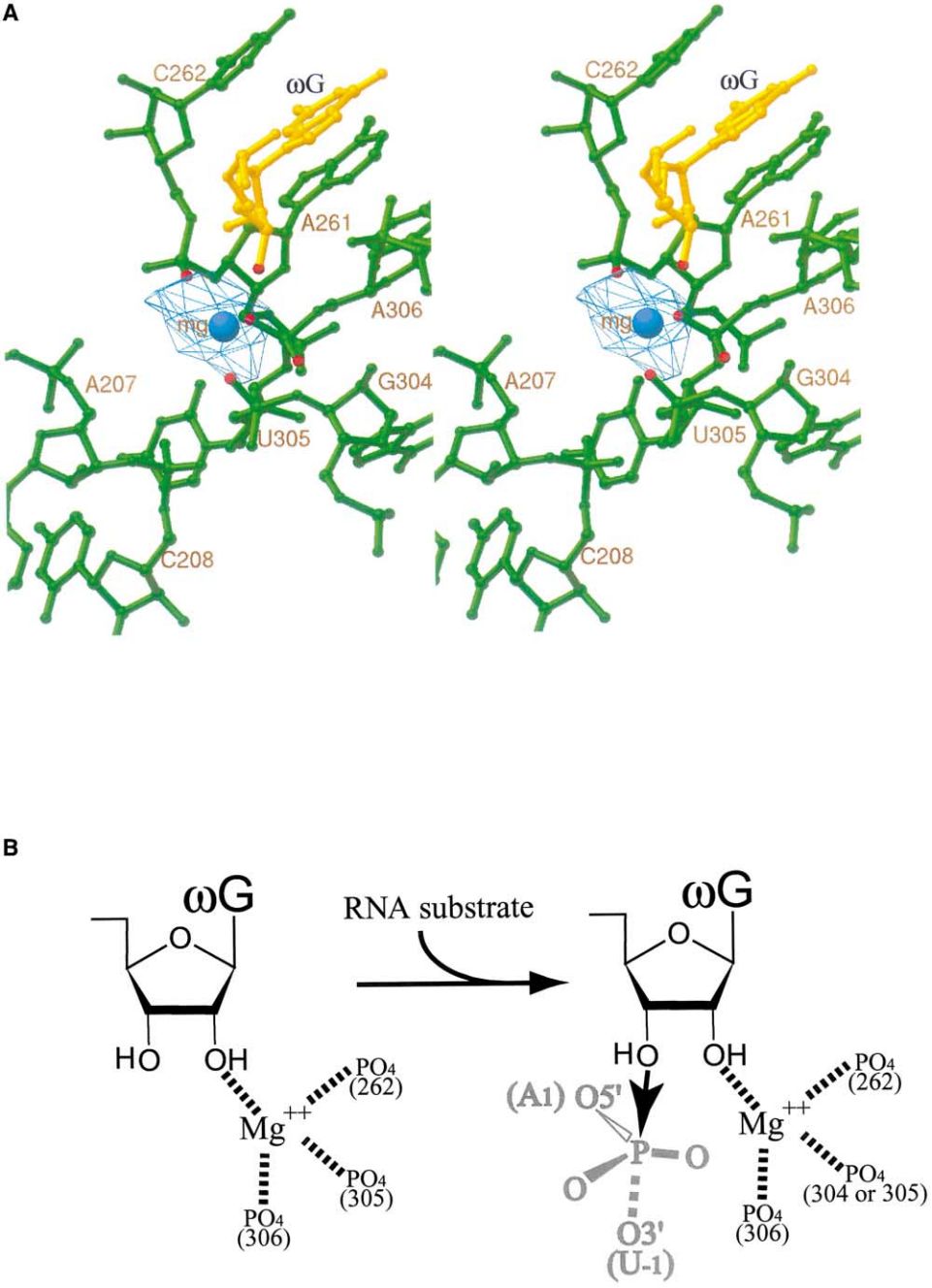

Figure 6. A Metal Ion at the Active Site

(A) The active site structure in the B molecule. The magnesium ion deduced from a strong Eu site is shown as a blue ball. The Eu anomalous electron density is contoured at 6 σ. The oxygen atoms on the three phosphates close to the magnesium ion are indicated as red.

(B) Proposed catalytic role of the magnesium ion prebound at the active site. In the presence of the substrate (represented by the structure of the cleavage site phosphate in the transition state in gray), the interaction between the metal ion and the 2′-OH of ωG orients the 3′-OH for nucleophilic attack (arrow). Dotted P…O bond, a bond half-broken in the transition state.

heated at 50°C for 5 min and allowed to cool in a heat block for 10 min at room temperature before adding 0.1 vol of 200 mM $MgCl_2$ to adjust the final $MgCl_2$ concentration to 25 mM.

The crystals were grown at 30°C in 4 days, using the standard hanging drop vapor diffusion method. The hanging drops typically contained 3 μl of annealed RNA mixed with 3 μl of 50 mM K cacodylate (pH 6.0), 19% 2-methyl-2,4-pentanediol (MPD), 50 mM KCl, 10 mM $MgCl_2$, and 0.5 mM spermine. Each well contained 1 ml of 50 mM Na cacodylate (pH 6.0) and 19%–23% MPD. The crystallization was not very reproducible and crystal morphology varied from batch to batch. Crystals were transferred to a stabilization solution, containing 50 mM K cacodylate (pH 6.0), 50 mM KCl, 50 mM $MgCl_2$, 25% MPD, 0.5 mM spermine, and 15% ethanol. The stabilization was performed at 30°C for at least 30 min before the crystals were either frozen in liquid nitrogen or transferred to heavy atom soak solution.

Crystals grew in the same form as that in the 5 Å structure determination (the "old form") (Golden et al., 1998), but underwent a lattice reorganization during stabilization in the presence of 15% ethanol to a "new form." Only the new form crystals diffracted to 3.8 Å resolution. During the lattice reorganization, the crystals cracked along planes perpendicular to the c axis and some healed completely (survived) within 20 min. The crystal dimension along the c axis also shrunk to about 3/4 of the original.

Native and derivative diffraction data were measured at the HHMI 8.2.1 and 8.2.2 beam lines at the Advanced Light Source (ALS) and processed using either DENZO and SCALEPACK or HKL2000 (Otwinowski and Minor, 1997). The requirement of lattice reorganization for high-resolution diffraction imposed strong constraints on data collection and structure determination. First, only crystals with cylindrical shapes and smaller than 200 μm survived the lattice reorganization. Only a small fraction of the surviving crystals were of data collection quality. Thus, about 1000 crystals had to be prepared for native and derivative data collection. Second, the small crystal size and weak diffraction made it necessary to perform long exposures to obtain high-resolution data, even with brilliant synchrotron X-ray beams. Crystals decayed during data collection and generally had a usable lifetime of 2000 s at these beam lines. As a result, diffraction limit and data quality were in competition. Third, crystals were generally not isomorphous to each other, even in the absence of heavy atom soaks. Therefore, anomalous signals were used as the only indication of potential derivatives.

Structure Determination and Refinement

Heavy atom derivatives were obtained by soaking the new-form crystals for 2 days in solutions containing 0.3 mM $EuCl_3$ or $DyCl_3$ or 1 mM Ir hexammine, in addition to the stabilizer components. Peak wavelengths were used for the Eu, Ir-1, and Dy-1 data sets. Subsequent to Dy-1, the same crystal was used to collect two additional data sets with wavelength alternating between the inflection point and high-energy remote at every 5° (Table 1). An exceptionally large Ir derivative crystal allowed collection of a multiple wavelength anomalous dispersion (MAD) data set (Ir-2, -3, -4) (Table 1).

Four strong Eu sites were initially identified using SHELX-D (Schneider and Sheldrick, 2002). Subsequent phased and crossphased anomalous difference maps permitted location of 22 additional Eu sites, as well as 28 Dy and 17 Ir sites. Isomorphous signals were not useful in phasing when they were from different crystals, because of nonisomorphism. Single-wavelength anomalous dispersion (SAD) phase refinement was individually performed for Eu, Ir-1, Dy-1, and Dy-2; similarly, single isomorphous replacement (SIR) refinement was performed for Dy-2 and Dy-3, and MAD phasing for Ir-2, Ir-3, and Ir-4. These phase sources were combined using amplitudes from the native data. Interestingly, two combinations of subsets of phase information (Eu/Ir-1; Dy-1/Dy-2/Dy-3/Ir-2/Ir-3/Ir-4) provided better electron density maps than the combination of all. Following density modification and phase extension, the maps generated from the two different combinations of phases were somewhat different from each other, and both were used in the initial RNA chain tracing.

The strongest Eu and Ir sites formed a triangle of interatomic distances, characteristic of those found between Eu and osmium hexammine sites in the P4-P6 domain structure (Cate et al., 1996). Since both Ir hexammine and osmium hexammine mimic hexahydrated magnesium ion in RNA structures, we assumed they bound to similar sites on the ribozyme. Four such Eu/Ir/Ir site triples were identified. The placement of the higher resolution P4-P6 domain structure according to these triangles allowed the determination of the space group as $P4_12_12$ and greatly facilitated the tracing. Noncrystallographic averaging caused the electron density to deteriorate. Therefore, noncrystallographic symmetry was not used in any stage of the structure determination and refinement. Heavy atom site refinement, phase combination, density modification, phase extension, and subsequent structure refinement were performed using CNS (Brunger et al., 1998).

The Truncate procedure in CCP4 was applied to the native data (CCP4, 1994; French and Wilson, 1978) and was found to produce more details in the electron density. B factor sharpening (Bass et al., 2002; DeLaBarre and Brunger, 2003) was also used to generate maps with more details, by applying the factor exp ($-B_{sharp} \times (s \times s)/4$) to the native amplitude. B_{sharp} values used in this work ranged from -40 to -113 Å^2. The P4-P6 domain regions were traced first, using the program "O" (Jones et al., 1991). The partial-model phases resulted in greatly improved electron density maps that allowed the tracing of the P3-P9 regions. The lower resolution Tet3-9 model was not used in the modeling.

Refinements were carried out using the MLHL target function (Adams et al., 1997) against truncated native amplitudes at 20–3.8 Å resolution and the combined experimental phase distributions (Eu/Ir-1). Weak Eu and Ir sites were identified using model-phased anomalous difference Fourier. Further rounds of SAD-phase refinement were carried out to generate a better experimental phase set. Refinement and model building were guided by crossvalidation using a 7% randomly selected subset of the diffraction data. Watson-Crick base pairing restraints were applied to the refinement. The atomic B factors were refined by assigning one B per residue. Bulk solvent correction (Jiang and Brunger, 1994) could not be successfully applied to the refinement. The final model contained residues 96–286 and 292–414 for molecules A and D; 96–414 for molecule B; and 96–286, 292–406, and 412–414 for molecule C. Figures 2, 3C, and 3D were prepared using the program Molscript (Kraulis, 1991). Figures 3B, 4, 5, and 6A were generated with RIBBONS (Carson, 1997). Supplemental Figure S1 was produced using the DDMP program from the Center for Structural Biology at Yale University, New Haven, CT. The structure has been deposited in the Protein Data Bank with access code 1X8W.

Acknowledgments

We thank Dr. Axel Brunger for advice on structure determination and refinement; Dr. Quentin Vicens for comments on the manuscript; Drs. Thomas Steitz, Alfonso Mondragón, Lin Chen, Rob Batey, Marcelo Sousa, and Ming Lei for helpful discussions; Elaine Podell and Steven Edwards for help at the synchrotron; and Art Zaug, Karen Goodrich, and James Stroud for technical support. We are grateful to the staff at the HHMI beam lines 8.2.1 and 8.2.2 of the Advanced Light Source for assistance in data collection. This work was supported by the Howard Hughes Medical Institute.

Received: July 19, 2004
Revised: August 13, 2004
Accepted: August 19, 2004
Published: November 4, 2004

References

Adams, P.D., Pannu, N.S., Read, R.J., and Brunger, A.T. (1997). Cross-validated maximum likelihood enhances crystallographic simulated annealing refinement. Proc. Natl. Acad. Sci. USA *94*, 5018–5023.

Adams, P.L., Stahley, M.R., Kosek, A.B., Wang, J., and Strobel, S.A. (2004). Crystal structure of a self-splicing group I intron with both exons. Nature *430*, 45–50.

Bass, B.L., and Cech, T.R. (1984). Specific interaction between the self-splicing RNA of *Tetrahymena* and its guanosine substrate: implications for biological catalysis by RNA. Nature *308*, 820–826.

Bass, B.L., and Cech, T.R. (1986). Ribozyme inhibitors: deoxyguanosine and dideoxyguanosine are competitive inhibitors of self-splicing of the Tetrahymena ribosomal ribonucleic acid precursor. Biochemistry *25*, 4473–4477.

Bass, R.B., Strop, P., Barclay, M., and Rees, D.C. (2002). Crystal structure of *Escherichia coli* MscS, a voltage-modulated and mechanosensitive channel. Science *298*, 1582–1587.

Been, M.D., and Perrotta, A.T. (1991). Group I intron self-splicing with adenosine: evidence for a single nucleoside-binding site. Science *252*, 434–437.

Bevilacqua, P.C., Johnson, K.A., and Turner, D.H. (1993). Cooperative and anticooperative binding to a ribozyme. Proc. Natl. Acad. Sci. USA *90*, 8357–8361.

Brunger, A.T., Adams, P.D., Clore, G.M., DeLano, W.L., Gros, P., Grosse-Kunstleve, R.W., Jiang, J.S., Kuszewski, J., Nilges, M., Pannu, N.S., et al. (1998). Crystallography & NMR system: a new

software suite for macromolecular structure determination. Acta Crystallogr. D Biol. Crystallogr. *54*, 905–921.

Burke, J.M., Esherick, J.S., Burfeind, W.R., and King, J.L. (1990). A 3′ splice site-binding sequence in the catalytic core of a group I intron. Nature *344*, 80–82.

Cannone, J.J., Subramanian, S., Schnare, M.N., Collett, J.R., D'Souza, L.M., Du, Y., Feng, B., Lin, N., Madabusi, L.V., Muller, K.M., et al. (2002). The Comparative RNA Web (CRW) site: an online database of comparative sequence and structure information for ribosomal, intron, and other RNAs. BMC Bioinformatics *3*, 2.

Carson, M. (1997). Ribbons. Methods Enzymol. *277*, 493–505.

Cate, J.H., and Doudna, J.A. (1996). Metal-binding sites in the major groove of a large ribozyme domain. Structure *4*, 1221–1229.

Cate, J.H., Gooding, A.R., Podell, E., Zhou, K., Golden, B.L., Kundrot, C.E., Cech, T.R., and Doudna, J.A. (1996). Crystal structure of a group I ribozyme domain: principles of RNA packing. Science *273*, 1678–1685.

Cate, J.H., Yusupov, M.M., Yusupova, G.Z., Earnest, T.N., and Noller, H.F. (1999). X-ray crystal structures of 70S ribosome functional complexes. Science *285*, 2095–2104.

CCP4 (Collaborative Computational Program, Number 4) (1994). The CCP4 suite: programs for protein crystallography. Acta Crystallogr. D Biol. Crystallogr. *50*, 760–763.

Christian, E.L., and Yarus, M. (1993). Metal coordination sites that contribute to structure and catalysis in the group I intron from *Tetrahymena*. Biochemistry *32*, 4475–4480.

Davies, R.W., Waring, R.B., Ray, J.A., Brown, T.A., and Scazzocchio, C. (1982). Making ends meet: a model for RNA splicing in fungal mitochondria. Nature *300*, 719–724.

DeLaBarre, B., and Brunger, A.T. (2003). Complete structure of p97/valosin-containing protein reveals communication between nucleotide domains. Nat. Struct. Biol. *10*, 856–863.

Doherty, E.A., Batey, R.T., Masquida, B., and Doudna, J.A. (2001). A universal mode of helix packing in RNA. Nat. Struct. Biol. *8*, 339–343.

Doudna, J.A., and Cech, T.R. (2002). The chemical repertoire of natural ribozymes. Nature *418*, 222–228.

Draper, D.E. (2004). A guide to ions and RNA structure. RNA *10*, 335–343.

Fedor, M.J. (2002). The role of metal ions in RNA catalysis. Curr. Opin. Struct. Biol. *12*, 289–295.

French, G.S., and Wilson, K.S. (1978). On the treatment of negative intensity observations. Acta Crystallogr. A *34*, 517–525.

Golden, B.L., Podell, E.R., Gooding, A.R., and Cech, T.R. (1997). Crystals by design: a strategy for crystallization of a ribozyme derived from the *Tetrahymena* group I intron. J. Mol. Biol. *270*, 711–723.

Golden, B.L., Gooding, A.R., Podell, E.R., and Cech, T.R. (1998). A preorganized active site in the crystal structure of the *Tetrahymena* ribozyme. Science *282*, 259–264.

Guerrier-Takada, C., Gardiner, K., Marsh, T., Pace, N., and Altman, S. (1983). The RNA moiety of ribonuclease P is the catalytic subunit of the enzyme. Cell *35*, 849–857.

Guo, F., and Cech, T.R. (2002). Evolution of *Tetrahymena* ribozyme mutants with increased structural stability. Nat. Struct. Biol. *9*, 855–861.

Jiang, J.S., and Brunger, A.T. (1994). Protein hydration observed by X-ray diffraction. Solvation properties of penicillopepsin and neuraminidase crystal structures. J. Mol. Biol. *243*, 100–115.

Jones, T.A., Zou, J.Y., Cowan, S.W., and Kjeldgaard (1991). Improved methods for building protein models in electron density maps and the location of errors in these models. Acta Crystallogr. A *47*, 110–119.

Joyce, G.F. (2004). Directed evolution of nucleic acid enzymes. Annu. Rev. Biochem. *73*, 791–836.

Juneau, K., and Cech, T.R. (1999). In vitro selection of RNAs with increased tertiary structure stability. RNA *5*, 1119–1129.

Juneau, K., Podell, E., Harrington, D.J., and Cech, T.R. (2001). Structural basis of the enhanced stability of a mutant ribozyme domain and a detailed view of RNA–solvent interactions. Structure *9*, 221–231.

Kraulis, P.J. (1991). Molscript: a program to produce both detailed and schematic plots of protein structures. J. Appl. Crystallogr. *24*, 946–950.

Kruger, K., Grabowski, P.J., Zaug, A.J., Sands, J., Gottschling, D.E., and Cech, T.R. (1982). Self-splicing RNA: autoexcision and autocyclization of the ribosomal RNA intervening sequence of *Tetrahymena*. Cell *31*, 147–157.

McConnell, T.S., Cech, T.R., and Herschlag, D. (1993). Guanosine binding to the *Tetrahymena* ribozyme: thermodynamic coupling with oligonucleotide binding. Proc. Natl. Acad. Sci. USA *90*, 8362–8366.

Michel, F., and Dujon, B. (1983). Conservation of RNA secondary structures in two intron families including mitochondrial-, chloroplast- and nuclear-encoded members. EMBO J. *2*, 33–38.

Michel, F., and Westhof, E. (1990). Modelling of the three-dimensional architecture of group I catalytic introns based on comparative sequence analysis. J. Mol. Biol. *216*, 585–610.

Michel, F., Hanna, M., Green, R., Bartel, D.P., and Szostak, J.W. (1989). The guanosine binding site of the *Tetrahymena* ribozyme. Nature *342*, 391–395.

Michel, F., Ellington, A.D., Couture, S., and Szostak, J.W. (1990a). Phylogenetic and genetic evidence for base-triples in the catalytic domain of group I introns. Nature *347*, 578–580.

Michel, F., Netter, P., Xu, M.Q., and Shub, D.A. (1990b). Mechanism of 3′ splice site selection by the catalytic core of the sunY intron of bacteriophage T4: the role of a novel base-pairing interaction in group I introns. Genes Dev. *4*, 777–788.

Nissen, P., Hansen, J., Ban, N., Moore, P.B., and Steitz, T.A. (2000). The structural basis of ribosome activity in peptide bond synthesis. Science *289*, 920–930.

Otwinowski, Z., and Minor, W. (1997). Processing of X-ray diffraction data collected in oscillation mode. Methods Enzymol. *276*, 307–326.

Piccirilli, J.A., Vyle, J.S., Caruthers, M.H., and Cech, T.R. (1993). Metal ion catalysis in the *Tetrahymena* ribozyme reaction. Nature *361*, 85–88.

Richards, F.M., and Kundrot, C.E. (1988). Identification of structural motifs from protein coordinate data: secondary structure and first-level supersecondary structure. Proteins *3*, 71–84.

Rupert, P.B., Massey, A.P., Sigurdsson, S.T., and Ferre-D'Amare, A.R. (2002). Transition state stabilization by a catalytic RNA. Science *298*, 1421–1424.

Schneider, T.R., and Sheldrick, G.M. (2002). Substructure solution with SHELXD. Acta Crystallogr. D Biol. Crystallogr. *58*, 1772–1779.

Shan, S.O., and Herschlag, D. (1999). Probing the role of metal ions in RNA catalysis: kinetic and thermodynamic characterization of a metal ion interaction with the 2′-moiety of the guanosine nucleophile in the *Tetrahymena* group I ribozyme. Biochemistry *38*, 10958–10975.

Shan, S., Yoshida, A., Sun, S., Piccirilli, J.A., and Herschlag, D. (1999a). Three metal ions at the active site of the *Tetrahymena* group I ribozyme. Proc. Natl. Acad. Sci. USA *96*, 12299–12304.

Shan, S.O., Narlikar, G.J., and Herschlag, D. (1999b). Protonated 2′-aminoguanosine as a probe of the electrostatic environment of the active site of the *Tetrahymena* group I ribozyme. Biochemistry *38*, 10976–10988.

Sjogren, A.S., Pettersson, E., Sjoberg, B.M., and Stromberg, R. (1997). Metal ion interaction with cosubstrate in self-splicing of group I introns. Nucleic Acids Res. *25*, 648–653.

Sontheimer, E.J., Sun, S., and Piccirilli, J.A. (1997). Metal ion catalysis during splicing of premessenger RNA. Nature *388*, 801–805.

Steitz, T.A. (1999). DNA polymerases: structural diversity and common mechanisms. J. Biol. Chem. *274*, 17395–17398.

Streicher, B., von Ahsen, U., and Schroeder, R. (1993). Lead cleavage sites in the core structure of group I intron-RNA. Nucleic Acids Res. *21*, 311–317.

Valadkhan, S., and Manley, J.L. (2001). Splicing-related catalysis by protein-free snRNAs. Nature *413*, 701–707.

Weinstein, L.B., Jones, B.C., Cosstick, R., and Cech, T.R. (1997). A second catalytic metal ion in group I ribozyme. Nature *388*, 805–808.

Yarus, M., Illangesekare, M., and Christian, E. (1991). An axial binding site in the *Tetrahymena* precursor RNA. J. Mol. Biol. *222*, 995–1012.

Yoshida, A., Sun, S., and Piccirilli, J.A. (1999). A new metal ion interaction in the *Tetrahymena* ribozyme reaction revealed by double sulfur substitution. Nat. Struct. Biol. *6*, 318–321.

Accession Numbers

The coordinates of the Tet3-9-R14C structure have been deposited in the Protein Data Bank under the ID code 1X8W.